Non-monotonous enzyme-assisted self-assembly profiles resulting from reaction-diffusion processes in host gels

Jean-Yves Runser, Miryam Criado Gonzalez, Fatima Fneich, Morgane Rabineau, Bernard Senger, Pierre Weiss, Loïc Jierry, Pierre Schaaf

Version of Record: https://www.sciencedirect.com/science/article/pii/S0021979722005458
Manuscript_c922418476f2f73da70c692e0dd74fc9

Non-Monotonous Enzyme-Assisted Self-Assembly Profiles Resulting from Reaction-Diffusion Processes in Host Gels

Jean-Yves Runser[a,b,c], Miryam Criado-Gonzalez[a,b,c], Fatima Fneich[d], Morgane Rabineau[a,b], Bernard Senger[a,b], Pierre Weiss[d], Loïc Jierry[c,*], Pierre Schaaf[a,b,c,**]

[a] *Institut National de la Santé et de la Recherche Médicale, INSERM Unité 1121, CRBS, 1 rue Eugène Boeckel, 67085 Strasbourg Cedex, France.*
[b] *Université de Strasbourg, Faculté de Chirurgie Dentaire, 8 rue Sainte Elisabeth, 67000 Strasbourg, France.*
[c] *Université de Strasbourg, CNRS, Institut Charles Sadron (UPR22), 23 rue du Loess, 67034 Strasbourg Cedex 2, BP 84047, France.*
[d] *Université de Nantes, ONIRIS, INSERM UMR 1229, 1place Alexis Ricordeau, 44042 Nantes, France ; UFR Odontologie, Université de Nantes, 44042, France ; CHU Nantes, PHU4 OTONN, 44042, Nantes, France.*

Abstract

Reaction-diffusion (RD) processes are responsible for surface and in-depth micropatterning in inanimate and living matter. Here we show that enzyme-assisted self-assembly (EASA) of peptides is a valuable tool to functionnalize host gels. By using a phosphatase distributed in a host hydrogel, the diffusion of phosphorylated peptides from a liquid/host gel interface leads to the spontaneous formation of a pattern of phosphorylated peptides self-assembly presenting at least two self-assembly maxima. Variation of enzyme and peptide concentrations change the pattern characteristics. When a peptide drop is deposited on a phosphatase functionalized gel, a self-assembly pattern also forms both along the gel-solution interface and perpendicular to the interface. This self-assembly pattern induces a local change of the gel mechanical properties measured by nanoindentation. Its appearance relies on the formation of self-

*Corresponding author
**Corresponding author
Email addresses: loic.jierry@ics-cnrs.unistra.fr (Loïc Jierry), schaaf@unistra.fr (Pierre Schaaf)

assembled structures by nucleation and growth processes which are static in the hydrogel. This process presents great similarities with the Liesegang pattern formation and must be taken into account for the functionalization of hydrogels by EASA. A mechanism based on RD is proposed leading to an effective mathematical model accounting for the pattern formation. This work highlights EASA as a tool to design organic Liesegang-like microstructured materials with potentials applications in biomaterials and artificial living systems design.
Keywords: enzyme-assisted self-assembly • hydrogel • reaction-diffusion • Liesegang-like process • micropatterning

1. Introduction

Enzymes constitute a powerful tool to induce self-assembly processes, since they can act on soluble molecules and transform them into poorly soluble hydrogelators which then self-assemble.[1] This process, called Enzyme-Assisted Self-Assembly (EASA), has received considerable attention over the last decade.[2, 3, 4] For example when Fmoc-FFpY (Fmoc: 9-Fluorenylmethoxycarbonyl; F: phenylalanine; Y: tyrosine; p: phosphate group) peptides are brought into contact with alkaline phosphatase (AP), it transforms them into Fmoc-FFY which self-assemble in the form of long fibers of a few nanometers in diameter.[5, 6, 7] Mainly studied in solution, EASA has also been developed by immobilizing the enzymes on surfaces of various kinds (planar surfaces, nanoparticles, porous materials).[5, 8, 9, 10, 11] Recently the supramolecular self-assembly of small low molecular weight hydrogelators has started to be investigated in host gels,[12, 13, 14] opening the route to a new method of functionalization of gels for tissue engineering applications for example. In the case of EASA, a host gel containing enzymes is brought into contact with the hydrogelator-precursor solution.[15, 16] These molecules diffuse into the gel, are transformed into hydrogelators and then self-assemble in the host gel. We have, for example, shown that Fmoc-FFpY brought into contact with a polyethylene glycol (PEG) gel functionalized with AP leads to the formation of self-assembled nanofibers in the host gel and to

an accompanying change in the mechanical properties of the hydrogel.[16] Even if such a self-assembly process must result from the interplay between reaction and diffusion (RD) processes, this aspect has not been investigated so far. RD processes are at the origin of a large number of patterns observed in nature in inanimate as well as in living matter.[17] Among them, Liesegang patterns [18] are the first that have been thoroughly investigated. First noticed in 1855 by F.F. Runge,[19] and rediscovered by Liesegang in 1896, a first explanation was given by Ostwald [20]. They are observed when a precipitation reaction is coupled with diffusion processes in the absence of convection. Typically, when a soluble salt, A, diffuses into a gel containing another soluble salt, B, and when in addition AB forms a weakly soluble salt, one can observe, at high enough electrolyte concentrations the formation of regular structures such as rings or bands highly concentrated in AB precipitate. The characteristics of these structures (band or ring spacing, width of the bands...) depend upon numerous parameters such as the concentrations of the diffusing species or their diffusion coefficients. It is worth noting that B is generally in much lower concentration than A. The formation of this precipitate induces a zone in the gel, near the interface, that is depleted chiefly in B. Then, when A diffuses into the gel, the salt concentrations in this zone are below the critical supersaturation degree at which precipitation starts. The critical degree of supersaturation is again reached further from the interface where the depletion of B is less pronounced leading to a new zone of AB formation. This precipitate formation again generates a new zone depleted in B. Because A continues to diffuse into the gel, this process is likely to take place further in the gel and eventually to produce additional bands. Since their discovery, impressive experimental achievements in the generation of Liesegang microstructured materials have been reported, mainly based on reactions involving inorganic species.[21, 22] Despite their huge implications in biology, investigations based on the self-assembly of purely organic systems are rare.[12, 13, 23, 24, 25] Here we will show that EASA taking place in enzyme functionalized host gels into contact with a precursor peptide solution leads to self-assembly patterns at the gel/solution interfaces. We will

investigate the characteristics of the pattern and propose a simple mechanistic model accounting for the main observed features.

2. Material and Methods

2.1. Experimental

2.1.1. Chemicals and abbreviations

Name, acronym (abbreviation)	MW (g/mol)	Supplier	CAS number	Purity
Alkaline Phosphatase (AP)	160000	Sigma Aldrich	9001-78-9	Used as purchased
Rhodamine-labeled Alkaline Phosphatase	Prepared according to ref. [26].			
Sodium tetraborate anhydrous (borax)	201.22	Acros Organics	1330-43-4	$\geq$ 98%
Hydroxypropylmethyl Cellulose Silanized (Si-HPMC)	Prepared according to ref. [27].			
Fmoc-FF*p*Y	700	Pepmic (Suzhou, China)	- -	$\geq$ 99%
4-(2-Hydroxyethyl)-1-Piperazineethanesulfonic Acid (Hepes)	238.305	Fisher Scientific	7365-45-9	$\geq$ 99%
Rhodamin B isothiocyanate (RHO)	536.08	Sigma Aldrich	36877-69-7	Used as purchased
Thioflavin T (ThT)	318.86	Sigma Aldrich	2390-54-7	$\geq$ 60%
p-Nitrophenyl Phosphate (pNPP)	263.05	Sigma Aldrich	4264-83-9	Used as purchased
Phosphate Buffered Saline Tablets	- -	Sigma	- -	Used as purchased
Sodium Chloride	58.44	Fisher Scientific	7647-14-5	$\geq$ 99.5%

2.1.2. Solutions and buffers preparation

The Hepes buffer solution (pH 3.6) was prepared by dissolving 3.1 g of Hepes and 1.46 g of sodium chloride in 100 mL MilliQ water. After 1 night stirring, the pH was adjusted to 3.6 using an HCl solution at 0.1 M.

The borax buffer solution (25 mM, pH 9.5) was prepared by dissolving 1 g of anhydrous sodium tetraborate in 200 mL MilliQ water. After 1 night stirring, the pH was adjusted by using a NaOH solution at 0.1 M.

The Phosphate Buffer Saline (PBS) solution (pH 7.4) was prepared by dissolving 1 tablet in 200 mL MilliQ water leading to a solution containing 0.01 M Phosphate Buffer, 0.0027 M potassium chloride and 0.137 M sodium chloride.

2.1.3. Host hydrogel cross-linking conditions and diffusion of Fmoc-FFpY within this host gel

Si-HPMC polymer chains and the host hydrogels made from Si-HPMC (called here HPMC gels) were prepared according to reference [27]. First, 6 g of Si-HPMC were dissolved in 194 mL of a NaOH solution at 0.2 M and stirred for 48 h. After complete dissolution, two dialysis baths were performed in NaOH solutions at 0.09 M. The first dialysis bath ran for 15-16 h while the second bath ran for 1-2 h. One obtain a Si-HPMC (3% wt) polymer solution (Si-HPMC-PS) at pH 12.9. HPMC gels were prepared by mixing Si-HPMC-PS with Hepes buffer solution (pH 3.6) in a mold at equivolume (100 µL/100 µL). AP-HPMC gels, *i.e.*, HPMC gels containing AP, were prepared by first dissolving AP in a vial with Hepes buffer (pH 3.6) at 0.5 $mg \cdot mL^{-1}$. This solution was then mixed with Si-HPMC-PS in a mold or a petri dish at equivolume: in the molds 100 µL/100 µL, in the petri dish 1 mL/1 mL. Once the host gel was fully cross-linked (after 48 h at room temperature), 50 µL of Fmoc-FF*p*Y at 2 $mg \cdot mL^{-1}$ in borax (25 mM, pH 9.5) was deposited on the surface of the AP-HPMC gels in the case of the mold or a 4 µL drop was deposited in the case of the petri dish. Peptides from these solutions diffused for 12 h at room temperature before further investigations. To avoid evaporation of the peptide solution during its diffusion within the hydrogel, the mold and petri dish were carefully covered

with parafilm. It was verified that the gel was still covered by a thin film of liquid before measurements.

2.1.4. UV/Vis spectroscopy

The enzymatic activity was measured in a microplate reader by UV spectroscopy (FLX-Xenius®, SAFAS, Monaco) using a 96-well plate. The AP activity of the AP-HPMC gel was measured by incubation of the substrate, para-nitrophenyl phosphate (PNP) (150 µL at 1 mM in Borax buffer). Concentration and volume ensured a large excess of substrate for the enzymatic reaction. PNP is a colorless aqueous solution (commercially available) which leads to para-nitrophenol, a yellow compound absorbing light at $\lambda = 405$ nm.

2.1.5. Rheology measurements

HPMC, AP-HPMC and AP-HPMC + FmocFFpY gels were prepared as follows:

- HPMC : in a mold, mixing of 100 µL Hepes buffer (pH 3.6) with 100 µL of Si-HPMC (3 %).
- AP-HPMC : in a vial, dissolve AP in Hepes buffer (pH 3.6) at 0.5 $\mathrm{mg \cdot mL^{-1}}$. Mixing in a mold of 100 µL of this last solution with 100 µL of Si-HPMC (3 %).
- AP-HPMC + Fmoc-FFpY : same procedure as AP-HPMC.

Subsequently, 50 µL of different Fmoc-FFpY solutions (1 or 5 $\mathrm{mg \cdot mL^{-1}}$) were put into contact with HPMC and AP-HPMC gels for 12 hours at room temperature. Rheological properties were measured with a Kinexus Malvern rheometer using a 10-mm diameter plate geometry and a 1.8-mm gap. Strain measurements were carried out from 0.01 % to 100 % at 1 Hz. Frequency sweeps were performed from 0.01 Hz to 20 Hz at fixed strain of 0.01 %. All graphs are given in Figure S1.

2.1.6. Nanoindentation measurements

Samples were prepared as follows: in a vial, we dissolved AP in Hepes buffer (pH 3.6). We mixed this latter solution with Si-HPMC (3%) in a petri dish (1 mL/1 mL). After 48 h cross-linking, we added a drop (4 µL) of Fmoc-FF*p*Y dissolved in borax (25 mM, pH 9.5) at 5 $mg \cdot mL^{-1}$.

After 12 h of diffusion of the peptide, the nanoindentation experiment was performed using a Chiaro nanoindenter (Optics11, The Netherlands) equipped with a sensor of 0.24 $N \cdot m^{-1}$ cantilever spring constant at the end of which a tip of 33-µm radius was positioned. Data were fitted using the Hertz model to determine the Young modulus of the material by using the software of the nanoindenter.

2.1.7. Confocal laser scanning microscopy

All solutions were prepared following the procedure described here by employing alkaline phosphatase labeled with rhodamine B (AP^{RHO}) instead of AP. Depending on the type of acquisition performed, the samples were prepared as follows:

- Kinetics : ThioflavinT-AP^{RHO}-HPMC gels named ThT-AP^{RHO}-HPMC were prepared by dissolving in Hepes buffer (pH 3.6) ThT at 0.5 $mg \cdot mL^{-1}$ and AP at 0.5 $mg \cdot mL^{-1}$. This solution was mixed with Si-HPMC (3%) at equivalent volumes (100 µL/100 µL) in a mold designed for confocal microscopy. After 48 h of gelation, the gel was placed under a microscope head and acquisition was launched in time series before addition of 50 µL Fmoc-FF*p*Y at 2 $mg \cdot mL^{-1}$ in borax (25 mM, pH 9.5).

- Profile views : In this case, we dissolved, in a vial, AP in Hepes buffer (pH 3.6) at 0.5 $mg \cdot mL^{-1}$. We then mixed 100 µL of this solution with 100 µL of Si-HPMC (3%) in a mold. After 48 h of gelation, we added 50 µL of peptide at 2 $mg \cdot mL^{-1}$ in borax (25 mM, pH 9.5) and let it diffuse for 12 h. 2 h before profile visualization, we added 50 µL of ThT at 0.5 $mg \cdot mL^{-1}$ in borax (25 mM, pH 9.5) for self-assembly revealing.

The images were acquired using an inverted LSM 710 confocal scanning microscope (Zeiss, Germany). The ZEN 2.0 software was used for image capture. Samples were excited using a laser at 458 nm for ThT or 561 nm for AP^{RHO}. Gels were imaged directly in their containing molds. An EC Plan-NeoFluar $10\times/0.3$ objective was used for imaging.

2.2. Simulation

All simulations were performed in 1D using the finite elements method encoded with the Python programming language. This simulation work is extensively described in SI.

3. Results and Discussion

3.1. Self-assembly pattern in the drop configuration

By studying the EASA in a host hydrogel, we first deposited a drop of a phosphorylated peptide Fmoc-FF*p*Y (Fig. 1a) onto a HPMC host gel[27] containing alkaline phosphatase, called AP-HPMC. Alkaline phosphatase (AP) is an enzyme that dephosphorylates Fmoc-FF*p*Y into Fmoc-FFY which is known to self-assemble in solution.[5, 6, 7] In the presence of Thioflavine T (ThT), a fluorescent marker of a Fmoc-FFY self-assembly,[16] we observed, unexpectedly and by serendipity, around the peptide drop, a non-monotonous self-assembly profile both along the gel-solution interface and perpendicular to this interface in the gel: a chalice shape made of a peptide self-assembly was generated which matches with the geometry of the initial deposited drop (Fig. 1b and Fig. 1c). The observation was made by confocal laser scanning microscopy (CLSM). We will now investigate the origin and characteristics of this pattern formation.

3.2. Rheology measurements in the drop configuration

The above mentioned non-monotonous self-assembly profiles should result in local variations of the gel mechanical properties. This has been verified by depositing a drop of Fmoc-FF*p*Y solution on the host gel and measuring radially,

along the host gel surface, its local mechanical properties using nanoindentation (Fig. 1c and 1d). The elastic modulus, *i.e.*, the Young modulus E, is increasing when passing from the depleted to the enriched zone of peptide self-assembly which correspond to $E \approx 300$ Pa and $E \approx 700$ Pa respectively. Remarkably, the length of the second maximum zone (≈ 800 µm) fits the length of the fluorescence emission zone observed by fluorescence microscopy. We also note that the value of the Young modulus measured in the depleted zone is equivalent to that of the naked AP-HPMC gel ($E \approx 3 \times G' \approx 300$ Pa, Fig. S1), showing the quasi-absence of peptide self-assembly in this area. In several previous work [10, 15] we have reported that the enzymatic dephosphorylation of Fmoc-FF*p*Y leads to self-assembled nanofibers of Fmoc-FFY. The resulting nanofibrous network is able to underpin a supramolecular hydrogel architecture. Thus, when this network is generated within a host hydrogel as described in our work, it leads to the formation of an interpenetrated network resulting in a change of the mechanical properties, as we observed. When the concentration of the precursor Fmoc-FF*p*Y peptide is increased, the resulting Young modulus of the hydrogel also increases (Fig. S1).

3.3. Self-assembly profile on a flat interface

To better understand the origin of this pattern we focused on host gel surfaces uniformly brought into contact with a Fmoc-FF*p*Y solution. Through the fluorescence intensity measured along the direction perpendicular to the gel/solution interface, we followed the formation of the localized Fmoc-FFY self-assembly in depth and over time. AP is the trigger of the Fmoc-FFY self-assembly. Using AP^{RHO},[26] we have checked the enzyme distribution before the deposition of Fmoc-FF*p*Y (Fig. 2a, $t = 0$ min): AP^{RHO} is homogeneously distributed all over the HPMC host gel, except a slight increase of enzyme density at the interface with the air, *i.e.*, at the top of the HPMC gel, as well as at the gel/lamella interface. The AP^{RHO} observed in Fig. S2 shows that the enzyme is diffusing in the gel. After deposition of a Fmoc-FF*p*Y solution on top of the gel (containing ThT) we observed the Fmoc-FFY self-assembly pattern

formation over time. The kinetics of the whole pattern formation is given in a time lapse video provided as supporting information (ESI, Video S1). Typical snapshots of this formation taken at 36 , 60 and 180 min after contact with the precursor peptide solution are given (Fig. 2a). Z-stacked images allow to rebuild the so-microstructured gel, showing the distribution of both the AP (red) and the Fmoc-FFY self-assembly (green) (Fig. 2b).

The monitoring of the evolution over time reveals that Fmoc-FFY self-assembly starts instantaneously at the interface between the gel and the precursor peptide solution. This spontaneous process is not due to the presence of the excess of enzymes located at the gel/air interface before the deposition of the Fmoc-FFpY solution because the removal of this excess of AP by rinsing has no significant effect on the resulting self-assembled pattern (Fig. S3). After $\approx$ 40 min of contact with the Fmoc-FFpY solution, a second maximum of Fmoc-FFY self- assembly appears in the host gel, located $\approx$ 500 µm from the interface (Fig. 2a/2b and Video S1). The self-assembly profile then decreases going from this second maximum to the bottom of the gel over a distance of $\approx$ 800 µm; $\approx$ 60 min are required to establish entirely the second maximum and the related self-assembly profile. A $\approx$ 400-µm thick zone almost totally depleted in Fmoc-FFY self-assembly is observed between the first and the second maxima. It is interesting to notice the asymmetric shape of the self-assembly in the host gel with a steep increase before reaching the secondary maximum and a slow decrease of the self-assembly concentration towards the end of the gel.

To prove that the existence of the green fluorescence profile is indeed due to the self-assembly process we replaced Fmoc-FFpY in the contacting solution by fluorescein diphosphate (FDP), a molecule that is dephosphorylated in the presence of AP and becomes fluorescent. Neither the depletion zone nor the two fluorescence maxima were observed (Fig. S4). To support these observations, we performed additional control experiments. The presence of self-assembled Fmoc-FFY was also confirmed by using the characteristic red shift fluorescence emission of the stacked Fmoc groups at λ_{em} = 315 nm due to the aromatic excimer formation when excited at λ_{ex} = 290 nm (Fig. S5).[28] The fact that

the appearance of green fluorescence in the host gel is due to the presence of a peptide self-assembly was verified by bringing a gel containing only AP into contact with a ThT solution and by bringing a gel containing ThT but devoid of enzymes into contact with a Fmoc-FFpY solution. In both cases no significant green fluorescence was detected.

3.4. Dependence of the self-assembly profile on peptide and enzyme concentrations

Next, we investigated the dependence of the self-assembly profile on the initial conditions. Increasing the concentration of Fmoc-FFpY in the solution from 0.25 , 0.50 to 1 $\mathrm{mg \cdot mL^{-1}}$, while the initial enzyme concentration is fixed (0.25 $\mathrm{mg \cdot mL^{-1}}$), results in keeping the position of the self-assembly maximum in the host gel almost fixed while increasing its density and extending further the self-assembly zone towards the bottom of the host gel. This was observed through ThT fluorescence emission (Fig. S6a and S6b). Increasing the enzyme concentration in the host gel from 0.12 , 0.25 to 0.5 $\mathrm{mg \cdot mL^{-1}}$ while fixing that of the deposited Fmoc-FFpY solution (1 $\mathrm{mg \cdot mL^{-1}}$) results in a diminution of the depletion zone width corresponding to the distance between the second self-assembly maximum in the gel and the interface (from 300 µm to 100 µm, Fig. S6c and S6d). A concomitant decrease of the self-assembly zone thickness inside the hydrogel is also observed.

3.5. Origin of the self-assembly pattern

The central question is why does a depleted zone appear in spite of the diffusion of Fmoc-FFpY through the gel and the presence of AP in this area? In other words, what is the origin of the maximum of self-assembly located within the host gel? The first reason could be the formation of a zone depleted in enzymes in the gel at the gel/solution interface. Such a zone exists and is due to the diffusion of the enzymes into the solution when the gel enters into contact with the solution (Fig. 2a & 2b). When one monitors the evolution of the enzyme profile as a function of time (Fig. 2a & 2b), one never and nowhere observes a total

depletion in enzymes. This implies that the dephosphorylation reaction should always take place and one should not observe areas that are totally depleted in self-assembly as it is the case (Fig. 2a & 2b). The formation of a zone depleted in enzymes is thus not at the origin of the self-assembly depletion zone. Another reason could be an inhibition of AP in this zone. Indeed, the dephosphorylation step is accompanied by the generation of protons and phosphate ions which are both inhibitors of AP. We have performed many investigations in this direction. These inhibitors, largely produced at the gel/solution interface, diffuse into the gel and should be more concentrated close to the hydrogel/solution interface during the first stages of the whole process. Yet, if this would be the case, increasing the initial Fmoc-FF*p*Y concentration would lead to a stronger inhibition of the self-assembly with a larger depletion zone which is not the case (Fig. S6a and S6b). Moreover, if the host AP-HPMC hydrogel is put into contact for 24 h with borax buffer (pH 9.5) or phosphate buffer (pH 7.6) the depletion zone is still observed. Thus, the production of phosphate ions or protons during the dephosphorylation step is not responsible of the depletion zone formation (Fig. S7). The depletion zone of self-assembly must thus have another explanation. We propose the following mechanism schematically represented in Fig. 3 based on a simulation discussed later and fully described in SI section 1. In solution, when the phosphorylated Fmoc-FF*p*Y is mixed with AP, the self-assembly of Fmoc-FFY requires a lag time (already reported in the literature) that is a feature of EASA.[29, 30, 31, 32, 33] This observation agrees with the requirement of a critical concentration of Fmoc-FFY to initiate its own self-assembly, a mechanism close to the nucleation step involved in a crystallization process. When the Fmoc-FF*p*Y solution is brought into contact with the AP-HPMC hydrogel (Fig. 3a, t_0), some AP diffuses from the gel into the solution and the critical Fmoc-FFY concentration threshold is reached very rapidly at the interface (Fig. 3a, t_1). Despite this self-assembly of Fmoc-FFY, Fmoc-FF*p*Y peptides diffuse into the host hydrogel and are gradually dephosphorylated enzymatically to form "free" Fmoc-FFY peptides, *i.e.*, in a non-assembled state. Yet the concentration of free Fmoc-FFY is still too low

to initiate the "nucleation" of the self-assembly thus allowing their diffusion in all directions *i.e.*, also towards the self-assembled peak (first maximum) at the gel/solution interface. There, they interact irreversibly with the self-assembled structure which acts as a sink for "free" peptides. Thus, the interplay between the different reaction and diffusion processes can explain the formation of a zone depleted in Fmoc-FFY self-assembly. But all Fmoc-FF*p*Y that diffuse into the host gel are not transformed enzymatically near the gel/solution interface. Some are transformed further away from the interface and cannot diffuse up to the interface (Fig. 3a, t_2). This then leads to the buildup of a Fmoc-FFY profile inside the gel that presents a maximum at a certain distance from the gel/solution interface. When the Fmoc-FFY concentration at this maximum reaches the critical self-assembly concentration, self-assembly starts (Fig. 3a, t_3). Because it takes place in the host gel, the self-assembled entities are fix in the gel and a self-assembly maximum builds up at this position. This self-assembly also captures "free" Fmoc-FFY peptides that are produced in the gel between the gel/solution interface and this self-assembly zone. This then accentuates the depletion zone (Fig 3a, t_4). We have developed a simple model that captures the main features of this process namely (Fig. 3b, Video S2 and section 1 in SI): (*i*) diffusion of enzymes and precursors, (*ii*) transformation of precursor molecules into "free" hydrogelators in the presence of enzymes, (*iii*) self-assembly of hydrogelators when reaching a critical "free" hydrogelator concentration, (*iv*) capturing of "free" hydrogelators by the self-assemblies. We assume that the peptide self-assemblies remain fix (*i.e.*, do not diffuse) and that the transformation of precursors into hydrogelators is more rapid in the solution than in the gel. This latter assumption seems reasonable since the presence of the host gel should somehow hinder the diffusion of the enzymes and the peptides in the gel compared to the solution. The model is given in more detail in SI. It must be kept in mind that it is not intended to reproduce in its full details the system under investigation, in particular to reproduce precisely the enzyme kinetics or the nucleation kinetics but only to capture the main ingredients of the process responsible for the formation of the self-assembly profile, *i.e.*, the

formation of two self-assembly maxima. It comes out that these assumptions lead to the buildup of a self-assembly peak at the gel/solution interface followed by a depletion zone and a self-assembly secondary maximum in the gel (Fig 3b). The model also predicts that, with specific kinetic parameters, increasing the initial peptide concentration can lead to the appearance of multiple self-assembly maxima (SI, section 1). Preliminary experimental results show indeed, that by increasing the Fmoc-FFpY concentration at 20 $\mathrm{mg \cdot mL^{-1}}$ one can observe the presence of two self-assembly maxima (Fig. 4) in the host gel. One should notice that this result is obtained in two different experimental setups; first in depth (3D) using a mold containing AP-HPMC host hydrogel fully covered by 50 µL of the Fmoc-FFpY solution at 20 $\mathrm{mg \cdot mL^{-1}}$ (Fig. 4a), but also in surface (2D) using a petri dish containing AP-HPMC host hydrogel on top of which a drop of Fmoc-FFpY solution (5 µL at 20 $\mathrm{mg \cdot mL^{-1}}$) is deposited leading to the formation of two concentric rings of self-assembly surrounding the drop (Fig. 4b).

This spatiotemporally controlled self-assembly process presents strong analogies with the one leading to Liesegang ring patterns which result from inorganic salts precipitation.[18, 34] The model that we have developped is also close to those developped to describe the formation of Liesegang pattern for inorganic systems.[35, 36] The similarity between our and the Liesegang pattern formation is that both are due to the formation of static objects by a nucleation and growth process. The main difference is that in the Liesegang processes the objects are due to the reaction between two entities forming the nuclei whereas in our case the enzymatic reaction forms one entity that is at the origin of the pattern formation. One-dimensional Liesegang processes usually result in the formation of Liesegang rings, *i.e.*, several maxima of inorganic material which is also the case in our system. It must also be noticed that even if Liesegang patterns are usually observed with inorganic salts, more rarely for organic systems,[12] they have never been reported for EASA processes. Our work thus opens the EASA processes to the field of Liesegang patterns in host materials.

4. Conclusion

We have found that an enzyme-assisted self-assembly (EASA) process taking place in a host gel results in the formation of a self-assembly pattern at the gel-solution interface when a precursor peptide solution contacts the gel. The self-assembly pattern appears also along the interface when a drop of precursor solution is deposited on top of the gel. This pattern formation along the interface is accompanied by a local change of the mechanical properties of the hydrogel which closely follows the self-assembly pattern. It results from the coupling between the diffusion of the precursor peptides into the gel, their enzymatic transformation into self-assembling peptides which still diffuse in the gel and self-assemble when they reach a critical local concentration through a nucleation and growth process. This self-assembly remains immobile in the gel. The growth leads to a local depletion of self-assembling building blocks and this is the principal ingredient of the pattern formation in addition to directional flow and low diffusion rate. This process resembles a Liesegang-type process discovered with inorganic salts.[18, 34, 35, 36] As in Liesegang's experiments, our two interacting molecules diffuse (precursor peptides and enzymes). Though, there is a main difference: in a Liesegang's experiment the two reagents are used up whereas in the present work only the phosphorylated peptides are consumed while the enzymes are not. Indeed, it comes out that the self-assembly location is not a mirror image of the enzyme location in the host gel, but that the complex reaction-diffusion processes must be taken into account to predict the final self-assembly pattern. We have developed a model, based on the processes supposed to be at the origin of our observations, and aimed at accounting for the gross features of our findings. To become quantitatively and not only qualitatively predictive, the model developed here has to be improved, with a special emphasis on predicting the "exact" form of the self-assembly pattern. Our finding allows to envisage a way to tune both the mechanical features and the chemistry as well, in the three dimensions of a material with a spatiotemporal control. This aspect is particularly appealing since new properties can raise

from the peptides self-assembled state. Indeed, catalytic or biological activities have been largely reported to emerge from supramolecular self-assemblies [3, 37] and thus opens new avenues for applications in the fields of chemosensors design, cell-related applications (3D cultures, cell adhesion), drug delivery and tissue engineering.

Conflicts of interest

There are no conflicts to declare.

Acknowledgements

This work was financially supported by the Agence Nationale de la Recherche (project "EASA" ANR-18-CE06-0025-03), the Fondation pour la Recherche en Chimie (Project number PSC-005), the Labex Chimie des Systèmes Complexes (Project number PSC-016). J.-Y. Runser acknowledges the Faculté de Chirurgie Dentaire from the University of Strasbourg for his PhD fellowship. The ICS microscopy platform and the ICS characterization platform are acknowledged.

References

[1] Z. Yang, H. Gu, D. Fu, P. Gao, J. K. Lam, B. Xu, Adv. Mater. 16 (2004) 1440–1444.

[2] R. J. Williams, R. J. Mart, R. V. Ulijn, Pept. Sci. 94 (2010) 107–117.

[3] X. Du, J. Zhou, J. Shi, B. Xu, Chem. Rev. 115 (2015) 13165–13307.

[4] J. Baillet, A. Gaubert, J. Verget, L. Latxague, P. Barthélémy, Soft Matter 16 (2020) 7648–7651.

[5] C. Vigier-Carrière, T. Garnier, D. Wagner, P. Lavalle, M. Rabineau, J. Hemmerlé, B. Senger, P. Schaaf, F. Boulmedais, L. Jierry, Angew. Chem. Int. Ed. 54 (2015) 10198–10201.

[6] W. Wang, J. Qian, A. Tang, L. An, K. Zhong, G. Liang, Anal. Chem. 86 (2014) 5955–5961.

[7] Z. Hai, J. Li, J. Wu, J. Xu, G. Liang, J. Am. Chem. Soc. 139 (2017) 1041–1044.

[8] R. J. Williams, A. M. Smith, R. Collins, H. Hodson, A. K. Das, R. V. Ulijn, Nat. Nanotechnol. 4 (2009) 19–24.

[9] M. P. Conte, J. K. Sahoo, Y. M. Abul-Haija, K. H. A. Lau, R. V. Ulijn, ACS Appl. Mater. Interf. 10 (2018) 3069–3075.

[10] M. Criado-Gonzalez, J. Rodon Fores, A. Carvalho, C. Blanck, M. Schmutz, L. Kocgozlu, P. Schaaf, L. Jierry, F. Boulmedais, Langmuir 35 (2019) 10838–10845.

[11] J. Rodon Fores, M. Criado-Gonzalez, A. Chaumont, A. Carvalho, C. Blanck, M. Schmutz, C. A. Serra, F. Boulmedais, P. Schaaf, L. Jierry, Angew. Chem. Int. Ed. 58 (2019) 18817–18822.

[12] M. Lovrak, W. E. J. Hendriksen, C. Maity, S. Mytnyk, V. van Steijn, R. Eelkema, J. H. van Esch, Nat. Commun. 8 (2016) 15317.

[13] L. Schlichter, C. C. Piras, D. K. Smith, Chem. Sci. 12 (2021) 4162–4172.

[14] H. S. Cooke, L. Schlichter, C. C. Piras, D. K. Smith, Chem. Sci. 12 (2021) 12156–12164.

[15] M. Criado-Gonzalez, B. Loftin, J. Rodon Fores, D. Vautier, L. Kocgozlu, L. Jierry, P. Schaaf, F. Boulmedais, E. Harth, J. Mater. Chem. B 8 (2020) 4419–4427.

[16] M. Criado-Gonzalez, J. Rodon Fores, D. Wagner, A. P. Schröder, A. Carvalho, M. Schmutz, E. Harth, P. Schaaf, L. Jierry, F. Boulmedais, Chem. Commun. 55 (2019) 1156–1159.

[17] I. R. Epstein, B. Xu, Nat. Nanotech. 11 (2016) 312–319.

[18] R. Liesegang, Naturwiss. Wochenschr. 11 (1896) 353–362.

[19] F. F. Runge, Self-Edited (1855) 69.

[20] W. Ostwald, *Lehrbuch der allgemeinen Chemie* (Engelman, Leipzig) (1897).

[21] V. Castets, E. Dulos, J. Boissonade, P. De Kepper, Phys. Rev. Lett. 64 (1990) 2953–2956.

[22] Y. Wei, S. Han, D. A. Walker, P. E. Fuller, B. A. Grzybowski, Angew. Chem. Int. Ed. 51 (2012) 7435–7439.

[23] T. S. Babicheva, A. A. Konduktorova, S. L. Shmakov, A. B. Shipovskaya, J. Phys. Chem. B 124 (2020) 9255–9266.

[24] S. N. Semenov, A. J. Markvoort, T. F. A. de Greef, W. T. S. Huck, Angew. Chem. Int. Ed. 53 (2014) 8066–8069.

[25] A. Padirac, T. Fujii, A. Estévez-Torres, Y. Rondelez, J. Am. Chem. Soc. 135 (2013) 14586–14592.

[26] D. Mertz, C. Vogt, J. Hemmerlé, J. Mutterer, V. Ball, J.-C. Voegel, P. Schaaf, P. Lavalle, Nat. Mater. 8 (2009) 731–735.

[27] C. Trojani, P. Weiss, J.-F. Michiels, C. Vinatier, J. Guicheux, G. Daculsi, P. Gaudray, G. F. Carle, N. Rochet, Biomaterials 26 (2005) 5509–5517.

[28] A. M. Smith, R. J. Williams, C. Tang, P. Coppo, R. F. Collins, M. L. Turner, A. Saiani, R. V. Ulijn, Adv. Mater. 20 (2007) 37–41.

[29] Z. Yang, B. Xu, Chem. Commun. (2004) 2424–2425.

[30] K. Thornton, Y. M. Abul-Haija, N. Hodson, R. V. Ulijn, Soft Matter 9 (2013) 9430–9439.

[31] X. Qin, W. Xie, S. Tian, J. Cai, H. Yuan, Z. Yu, G. L. Butterfoss, A. C. Khuong, R. A. Gross, Chem. Commun. 49 (2013) 4839–4841.

[32] R. J. Williams, J. Gardiner, A. B. Sorensen, S. Marchesan, R. J. Mulder, K. M. McLean, P. G. Hartley, Aust. J. Chem. 66 (2013) 572–578.

[33] C. Vigier-Carrière, D. Wagner, A. Chaumont, B. Durr, P. Lupattelli, C. Lambour, M. Schmutz, J. Hemmerlé, B. Senger, P. Schaaf, F. Boulmedais, L. Jierry, Langmuir 33 (2017) 8267–8276.

[34] R. Sultan, P. Ortoleva, F. DePasquale, P. Tartaglia, Earth-Sci. Rev. 29 (1990) 163–173.

[35] H. Nabika, M. Itatani, I. Lagzi, Langmuir 36 (2020) 481–497.

[36] A. A. Polezhaev, S. C. Müller, Chaos 4 (1994) 631–636.

[37] O. Zozulia, M. A. Dolan, I. V. Korendovych, Chem. Soc. Rev. 47 (2018) 3621–3639.

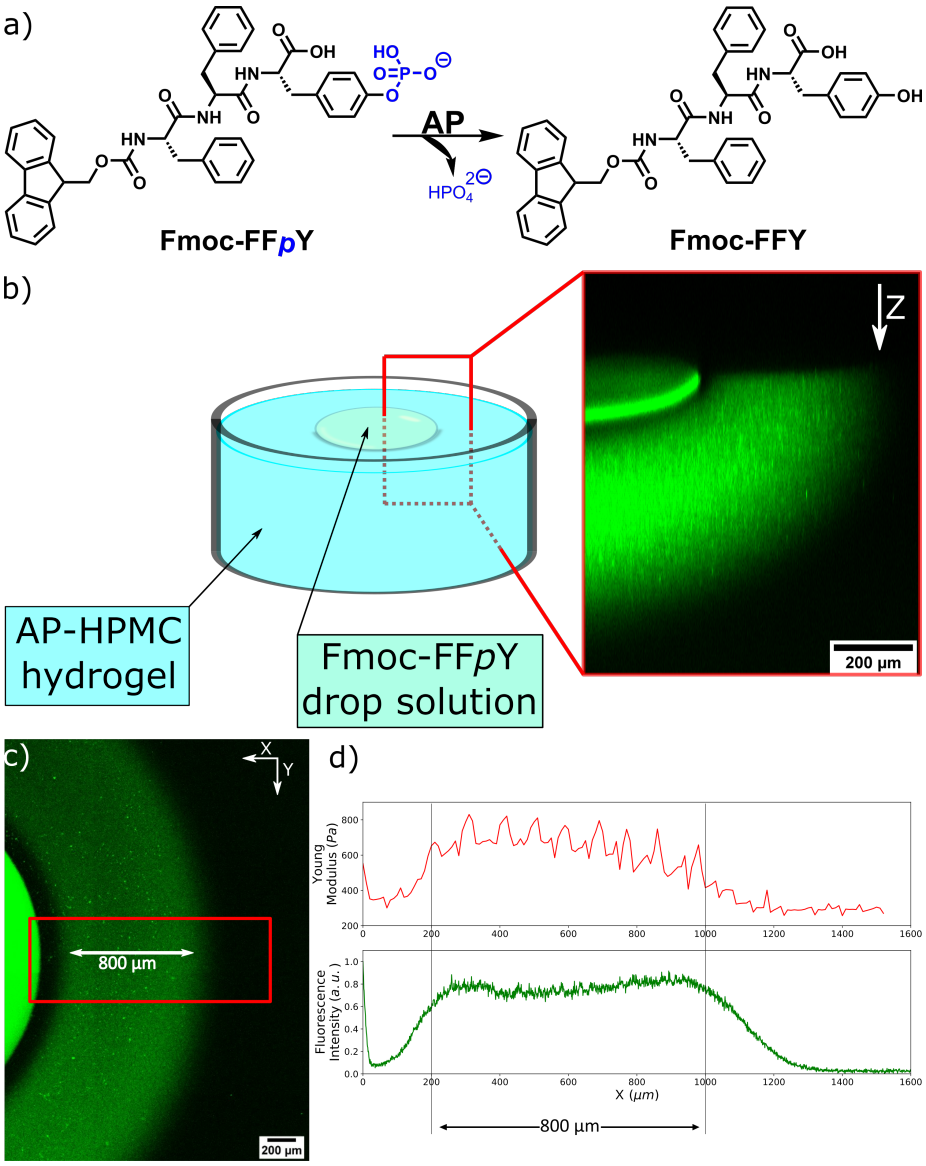

Figure 1: (a) Enzymatic hydrolysis of Fmoc-FFpY in Fmoc-FFY in presence of AP. (b) Cross-sectional view and (c) top view of the AP-HPMC hydrogel observed by CLSM, 12h after the drop deposition of Fmoc-FFpY solution. ThT was used to reveal the Fmoc-FFY β-sheet assemblies through their green fluorescence emission. The red box in (c) corresponds to the area analyzed by (d) nanoindentation (top) and fluorescence emission measurements (bottom).

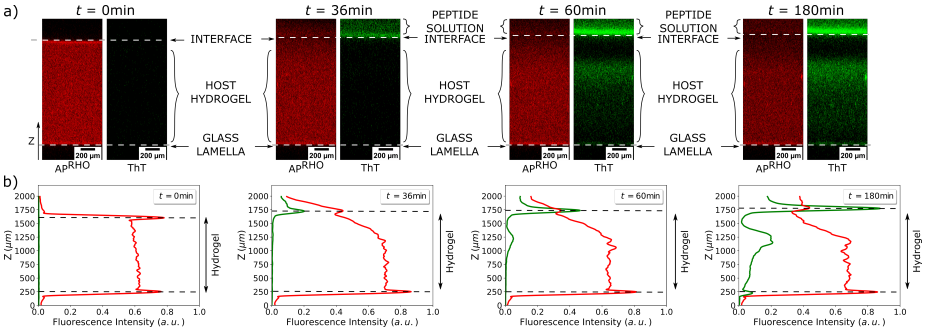

Figure 2: (a) Evolution of both the AP^{RHO} distribution (red) and the Fmoc-FFY self-assembly through ThT fluorescence emission (green) within an enzymatically active HPMC host hydrogel over time: $t = 0$ means before the deposition of the precursor peptide Fmoc-FFpY solution on top of the host hydrogel; : $t = 36$, 60 and 180 mean the time in min elapsed after the Fmoc-FFpY solution deposition. (b) Cross-section profiles of the host hydrogel showing the relative fluorescence intensity of AP^{RHO} and ThT at $t = 0$, 36 , 60 and 180 min.

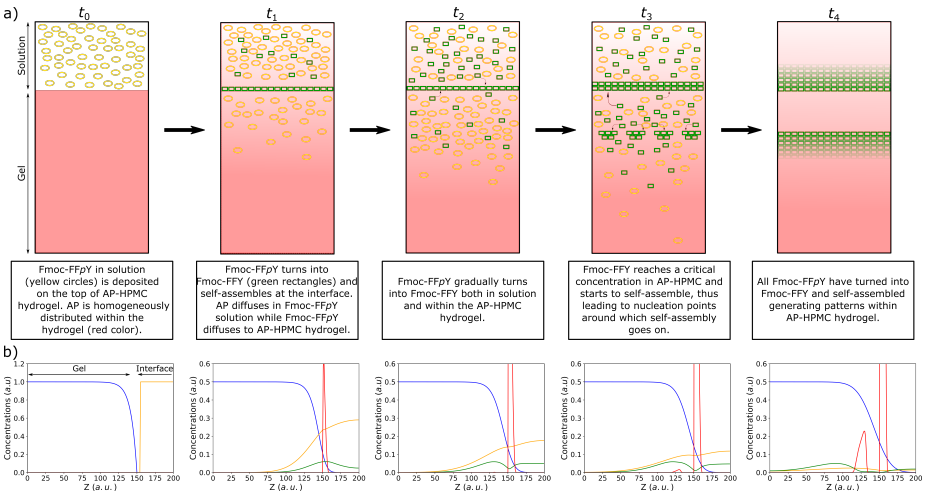

Figure 3: (a) Schematics of the mechanism of Fmoc-FFY self-assembly maximum formation within AP-HPMC hydrogel over time, going from t_0 to t_4.(b) is showing the simulations of relative concentration of AP (blue), precursor Fmoc-FFpY (orange), free hydrogelator Fmoc-FFY (green) and self-assembled Fmoc-FFY (red) over time, corresponding t_0, t_1, t_2, t_3 and t_4.

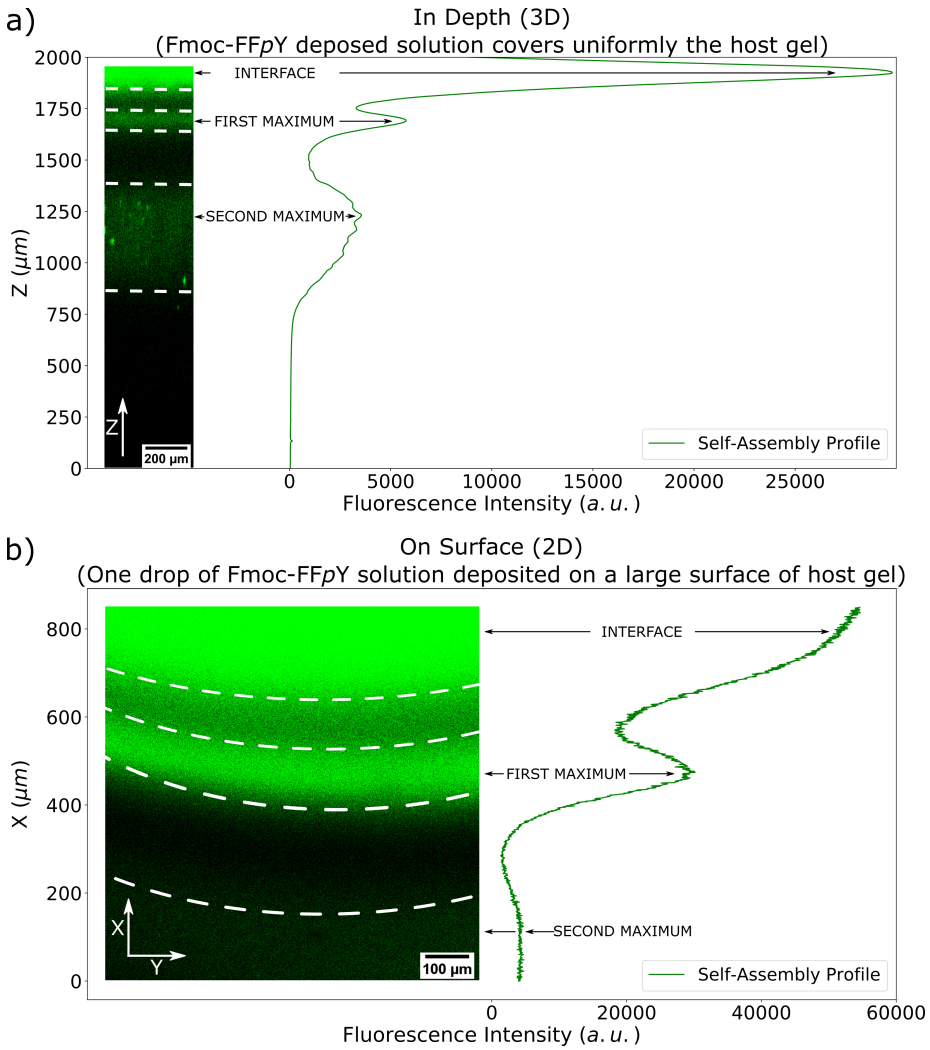

Figure 4: (a) Cross-sectional and (b) surface view of the self-assembly profile where the high concentration of Fmoc-FFpY (20 mg $\cdot$ mL^{-1}) allows the formation of two maxima in the host hydrogel.